Science Bulletin 65 (2020) 201–207

Contents lists available at ScienceDirect

Science Bulletin

journal homepage: www.elsevier.com/locate/scib

Article

Inhomogeneous-strain-induced magnetic vortex cluster in one-dimensional manganite wire

Iftikhar Ahmed Malik [a,1], Houbing Huang [b,1], Yu Wang [c,1], Xueyun Wang [d], Cui Xiao [e], Yuanwei Sun [f], Rizwan Ullah [a], Yuelin Zhang [a], Jing Wang [a], Muhammad Abdullah Malik [a], Irfan Ahmed [a], Changmin Xiong [a,*], Simone Finizio [g,h], Mathias Kläui [g,h], Peng Gao [f,i], Jie Wang [c,*], Jinxing Zhang [a,*]

[a] Department of Physics, Beijing Normal University, Beijing 100875, China
[b] Advanced Research Institute of Multidisciplinary Science, Beijing Institute of Technology, Beijing 100081, China
[c] Department of Engineering Mechanics & Key Laboratory of Soft Machines and Smart Devices of Zhejiang Province, Zhejiang University, Hangzhou 310027, China
[d] School of Aerospace Engineering, Beijing Institute of Technology, Beijing 100081, China
[e] Department of Physics, University of Science and Technology Beijing, Beijing 100083, China
[f] International Center for Quantum Materials and Electron Microscopy Laboratory, School of Physics, Peking University, Beijing 100871, China
[g] Department of Physics, Johannes Gutenberg-University Mainz, Mainz 55099, Germany
[h] Graduate School of Excellence Materials Science in Mainz, Mainz 55128, Germany
[i] Collaborative Innovation Center of Quantum Matter, Beijing 100871, China

ARTICLE INFO

Article history:
Received 18 August 2019
Received in revised form 23 October 2019
Accepted 12 November 2019
Available online 27 November 2019

Keywords:
Magnetic vortex cluster
Inhomogeneous strain
One-dimensional manganites
Epitaxial thin films
Cryo-Temperature MFM

ABSTRACT

Mixed-valance manganites with strong electron correlation exhibit strong potential for spintronics, where emergent magnetic behaviors, such as propagation of high-frequency spin waves and giant topological Hall Effects can be driven by their mesoscale spin textures. Here, we create magnetic vortex clusters with flux closure spin configurations in single-crystal $La_{0.67}Sr_{0.33}MnO_3$ wire. A distinctive transformation from out-of-plane domains to a vortex state is directly visualized using magnetic force microscopy at 4 K in wires when the width is below 1.0 μm. The phase-field modeling indicates that the inhomogeneous strain, accompanying with shape anisotropy, plays a key role for stabilizing the flux-closure spin structure. This work offers a new perspective for understanding and manipulating the non-trivial spin textures in strongly correlated systems.

1. Introduction

Topologically stabilized magnetic spin structures at the nanoscale, including domain walls [1,2], vortices [3,4] and skyrmions [5–9], have recently received much attention where structure and dynamics of sub-micrometer magnetic domains are the main factors determining the physical properties and applications. In magnetic materials, due to the competition between different energy contributions such as magnetocrystalline anisotropy, magnetoelastic coupling, or dipole interactions, there naturally exist nanoscale non-linear spin textures such as magnetic domain walls, magnetic vortex and magnetic skyrmions [10–13]. Among them, the vortex is a typical and well-known magnetic domain structure in dimensionally confined structures with a symmetry determined by its polarity and chirality [3,14,15]. Because of its stability at the nanoscale [15] and its robust control on nanosecond timescales [16], the magnetic vortex can be a promising candidate for next-generation magnetic data-storage devices. So far vortices have been primarily studied in conventional 3d magnetic metals.

More exciting materials include strongly correlated electron systems, where manganites attract broad interest due to the discovery of colossal magneto resistance [17,18]. Many interesting phenomena were found to be associated with the tuning of magnetic structures, such as the magnetoresistance [19], domain-wall motion twisted by biased tip [20], the high-frequency spin-wave propagation [21], etc. Recently, a giant topological hall effect stemming from non-trivial spin textures was discovered in a manganite [22], confirming the important role of the electronic correlation in the topological properties. Spin structures in manganites are sensitive to various external stimuli such as strain [23], size [24], electric/magnetic fields [25], etc., making them a model system to study generation and manipulation of the non-trivial spin textures. However, magnetic vortices were only usually observed in spatially

* Corresponding authors.
E-mail addresses: cmxiong@bnu.edu.cn (C. Xiong), jw@zju.edu.cn (J. Wang), jxzhang@bnu.edu.cn (J. Zhang).
[1] These authors contributed equally to this work.

https://doi.org/10.1016/j.scib.2019.11.025
2095-9273/

confined nanostructures with a high symmetry such as the square-shaped, triangle-shaped, and disc-shaped nano-islands [3,4,15], and the shape-induced magnetic anisotropy is assumed to be the dominant mechanism for the formation of the magnetic vortex [3]. Moreover, the magnetic vortex in those isolated devices will limit the study on their dynamic interaction at mesoscales and so far the properties of close packed assemblies of vortices have not been studied.

Here, we report on generation of magnetic vortex clusters in one-dimensional $La_{0.67}Sr_{0.33}MnO_3$ (LSMO) wires, wherein the magnetic vortex clusters are directly observed using variable-temperature magnetic force microscopy (VT-MFM) as well as magnetoresistance measurements. To identify the origin of the stability of these clusters, we carried out phase-field modeling. We find that the vortex states in this one-dimensional manganite originate from the inhomogeneous strain coupled with its shape anisotropy, where a strain-mediated phase diagram was revealed.

2. Experiments

The LSMO wires were fabricated from the epitaxially grown LSMO thin film by electron beam lithography (EBL) (JEOL JBX6300FS) with Ar^+ etching. The epitaxial LSMO thin films with thickness of 100 nm were grown on (0 0 1) oriented $LaAlO_3$ (LAO) substrate by pulsed laser deposition (PLD) [26] (see Fig. S1 online). To study the size dependent effect on the magnetic structure, the LSMO wires were patterned into rectangular shapes with a length of 100 μm and different widths of 0.5 and 1.0 μm. The structural, macroscopic magnetic and electrical properties of the samples were characterized by X-ray diffraction (XRD), high-angle annular dark-field (HAADF) scanning tunneling electron microscopy (STEM), superconducting quantum interference device (SQUID) magnetometry, and Quantum design physical property measurement system (PPMS), respectively. The local magnetic images were obtained in VT-MFM [27,28]. To understand the formation of the magnetic spin structures, the influences of size and strain on the magnetic structure were investigated by a phase field model [29].

3. Results and discussion

Before patterning the LSMO wires, the quality and various physical properties of epitaxial LSMO thin film grown on LAO were characterized. The XRD spectrum of the LSMO film is shown in Fig. S1a (online), revealing high quality epitaxial/impurity-free growth of thin film. XRD also shows an elongation of out-of-plane lattice constant, which suggests the biaxial compressive strain on the film, triggered by the lattice mismatch between the LSMO and LAO (LSMO, cubic, 3.88 Å; LAO, cubic, 3.79 Å) [26,30]. Quality of thin film was further supported by HAADF-STEM image which shows the sharp interface between LSMO film and LAO substrate and defect- & impurity-free epitaxial growth of LSMO thin film on LAO substrate (Fig. S1c online). Furthermore, energy dispersive X-ray (EDX) spectroscopy images for LSMO/LAO thin film were recorded. Lanthanum, Oxygen, Manganese, Aluminum and Strontium are detected and highlighted by different colors which also supports impurity free growth of LSMO thin film (Fig. S2 online). The magnetic and resistive measurements show that the LSMO thin film exhibits a ferromagnetic metallic (FMM) behavior with a Curie temperature above 350 K (Fig. S4a online). Furthermore, the perpendicular magnetic anisotropy of the LSMO can be confirmed by analyzing the in-plane and out-of-plane field dependent magnetization (*M-H*) curves with a correction of the demagnetization effect (Fig. S4c and d online). All above mentioned physical properties of the LSMO films are consistent with previous reports [26].

It is well accepted that the magnetoelastic effect associated with substrate induced compressive strain gives rise to the occurrence of the perpendicular magnetic anisotropy [20,26]. According to the *M-H* curves, the effective magnetic anisotropy constant (K_{eff}) can be calculated [31]. The result shows an increase of K_{eff} when temperature decreases, similar to the dependence of saturation magnetization (M_S) on temperature (Fig. S4b online), indicating the enhancement of the magnetoelastic energy at low temperature. At 300 K, magnetic domains of LSMO are mobile, quickly settling into a labyrinthine-like pattern, but at 4 K, they enter into a randomly distributed state (see the MFM image in Fig. 1a and b respectively), which can be well reproduced using phase field modeling (Fig. S5 online). According to the modeling, the random distributed magnetic domain is due to the larger M_S and K_{eff} at low temperature. Fig. 1c shows MFM images for magnetization reversal process at 4 K, from fully upward saturated magnetization state to randomly distributed magnetic domain state at remanence. For external magnetic fields $H > 0.7$ T, no red regions are visible in the MFM images, indicating the system is fully saturated (single domain state). The red bubble observed is resulting from the impurity or particle on thin film surface. At 0.5 T, domains with downwards magnetization starts to nucleate, represented by light red regions. As the field further decreases, the down domains expand and the up domains shrink. In the absence of external magnetic field, almost equally populated up and down domains were formed, confirming the demagnetization state. The FM domain behavior is in excellent agreement with the *M-H* curve (Fig. 1d), suggesting the local observation is representative of the magnetic behavior of the entire film. Inset of Fig. 1d shows a comparison of the *M-H* curves of LSMO thin film taken at different temperatures.

The domain configuration of a magnetic material is determined by the balance of the anisotropy energies such as magnetocrystalline, magnetoelastic, shape-induced anisotropy, etc. Therein, strain and geometric size of the material are the two critical factors. By using the method described above, we successfully obtained and analyzed LSMO wires with different widths. 2D finite element analysis was employed to model the strain distribution in cross section of the LSMO wires, to understand the evolution of the magnetic structure. Compressive strain is applied at the bottom interface of the specimens to describe the misfit strain from substrate. The magnitude of the in-plane compressive strain is set at –2.37%, which was obtained from the XRD results. Fig. 2a shows the cross-sectional strain distributions of LSMO wires with the widths of 0.5, 1.0 and 2.0 μm, respectively. The results show that the strain in the $\boldsymbol{x}_2$ direction (ε_{22}) is almost fully relaxed at the two top corners, due to the traction-free boundary conditions on the top surface and both sides. Furthermore, the strain relaxation is highly dependent on the width of the wire. The strain distribution is extremely inhomogeneous for the 0.5 μm wide wire, but almost homogeneous for 1.0 and 2.0 μm wires (Fig. 2a). Calculated line profiles of ε_{22} along the normalized position of the top surface of LSMO wires with different widths are shown in Fig. 2b. The results indicate that the entire area of the wires with the width greater than 2.0 μm is fully strained, similar to the case in the continuous thin film, while the strain relaxation become more obvious with the decrease of the width and fully relaxed with width below 0.3 μm. It is worth noting that the strain in the $\boldsymbol{x}_1$ direction (ε_{11}) of all the LSMO wires always remains the same as that of the continuous film, which implies that the symmetry of the strain in the LSMO wires is broken. Therefore, the strains in $\boldsymbol{x}_1$ and $\boldsymbol{x}_2$ directions in wires can be considered as two independent parameters that could be used to tune the magnetic structure. Strain can be released on fabrication of submicron- or nano-structures on strained thin films, which results in the change of *c* lattice constant

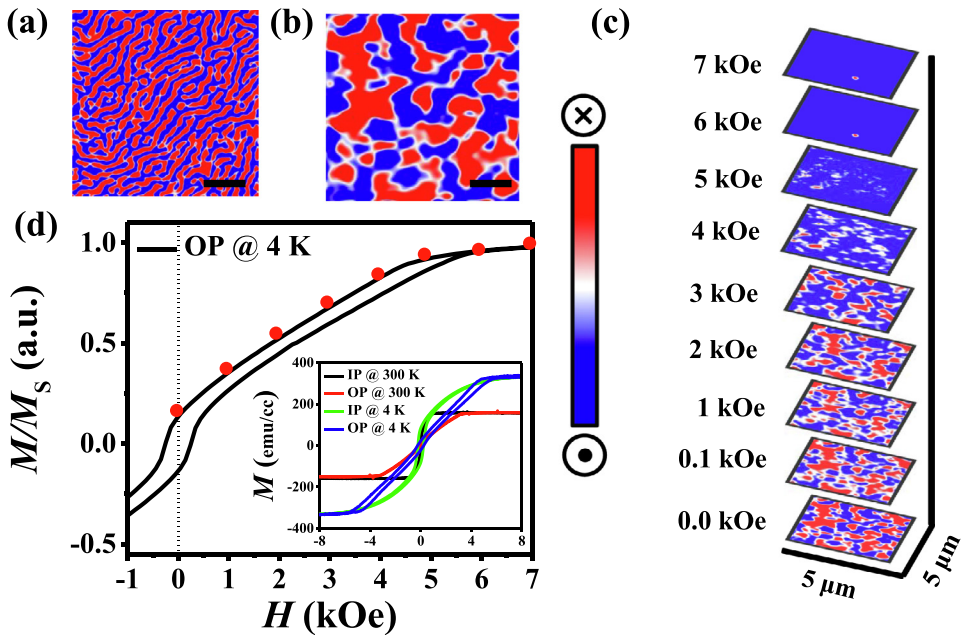

Fig. 1. (Color online) Magnetic domains and Magnetization reversal process in LSMO films. (a, b) MFM images taken at 300 and 4 K, respectively. (c) Direct imaging of magnetization reversal process from saturation state. (d) *M-H* curve recorded while external field is applied perpendicularly upward to thin film surface. Red dots on curve show the field where MFM images were recorded. Inset is *M-H* curves at different temperatures recorded by applying magnetic field parallel and perpendicular to thin film surface. Scale bar in (a, b) is 1.0 μm.

accordingly. So the variation of *c* lattice constant is a signature of the strain distribution, which could be revealed by XRD in term of observing the peak shift in LSMO which is an effective way to study the original strain state in the wire without breaking the structure. To analysis the strain, we have fabricated a sample as shown in schematics in Fig. S2b (online). Half of sample is fabricated into large number of 1D LSMO wires (100 μm × 500 nm × 100 nm), and the other half is remained as continuous thin film. Comparing the XRD data between thin film only and half film half wires sample, a clear extra peak of LSMO near the LAO peak is observed (Fig. S2a online), which is due to the reduction in *c* lattice from the half wires region. Furthermore, clear peaks of LSMO provide clear insight that LSMO is grown epitaxially on LAO substrate and lattice mismatch calculations for thin film (ε = –2.37%) and 1D wires (ε = –1.7%) are consistent with phase field modeling.

MFM was employed to study the domain configuration of the patterned LSMO wires at 4 K. Fig. 2c and f shows the topographic images of the 0.5 and 1.0 μm wide wires, revealing an atomically flat surface. Fig. 2d and g show the typical MFM images at 4 K on 0.5 and 1.0 μm wide wires, respectively. The MFM image for the 1.0 μm wide wire reveals random out-of-plane domain state, similar to continuous thin film. However, MFM for the 0.5 μm wide wire displays a flux closure domain configuration, showing the presence of magnetic vortex. To rule out any fast scanning axis effect on MFM image of vortex cluster state, MFM was performed on LSMO 0.5 μm wide wire in different directions. All images are giving the same results (Fig. S6 online).

To understand the formation of these spin structures, a phase field model is employed to analyze the domain configuration observed experimentally by MFM which is based on the time-dependent Ginzburg-Landau (TDGL) equation [29], in which different domain configurations are obtained through the minimization of the total free energy in the materials. To describe the strain-modulated domain configurations, the magnetoelastic coupling energy is included in the total free energy of the phase field model. The magneto-elastic coupling energy describes the coupling between strain components ε_{ij} and magnetization components M_i in the materials, which can be expressed in Eq. (1).

$$E_{\text{cou}} = -\frac{3\lambda_{100}}{2M_s^2}(c_{11}-c_{12})\left(\varepsilon_{11}M_1^2+\varepsilon_{22}M_2^2+\varepsilon_{33}M_3^2\right) - \frac{6\lambda_{111}}{M_s^2}c_{44}(\varepsilon_{12}M_1M_2+\varepsilon_{13}M_1M_3+\varepsilon_{23}M_2M_3), \quad (1)$$

where, c_{11}, c_{12} and c_{44} are the elastic constants, λ_{100} and λ_{111} are the magnetostrictive constants. The inhomogeneous strain in the LSMO wires is obtained by solving the mechanical equilibrium equation in the phase field model [29]. In addition to the magneto-elastic coupling energy, the total free energy used in the phase field model also includes the exchange energy, magnetic energy, pure elastic energy and magnetocrystalline anisotropy energy. The detailed formula of the total free energy is given in the Supplementary materials. From Fig. 2e and h it can be seen that, for the 0.5 and 1.0 μm samples, the configuration of the vortex and random domains are well reproduced theoretically. The underlying mechanisms will be discussed in a later section.

Temperature dependent magnetization (*M-T*) and resistance (*R-T*) measurements were performed for 0.5 μm wide wire (Fig. 3a). These measurements reveal an FMM, which is similar to the continuous LSMO thin film (Fig. S4a online). Fig. 3b shows the dependence of resistance of 0.5 μm wide wire on external magnetic field ($R_{xx}(H)$) applied perpendicularly to the surface at 4 K after ZFC. This curve shows typical features associated with the nucleation and annihilation of vortices [4]. As the external magnetic field reduces from saturation field, an abrupt change in resistance occurs near ± 1 kOe, which corresponds to the vortex nucleation. While the field increases, the resistance decreases gradually as the center of vortex approaches the wire edges and annihilates steadily. It is observed that this typical feature persists up to 100 K (Fig. S7 online). The corresponding annihilation and nucleation process of vortex in 0.5 μm wide bar has been captured using MFM imaging as shown in Fig. 3e, which agrees well with the $R_{xx}(H)$ results. It is also interesting that, after removing external

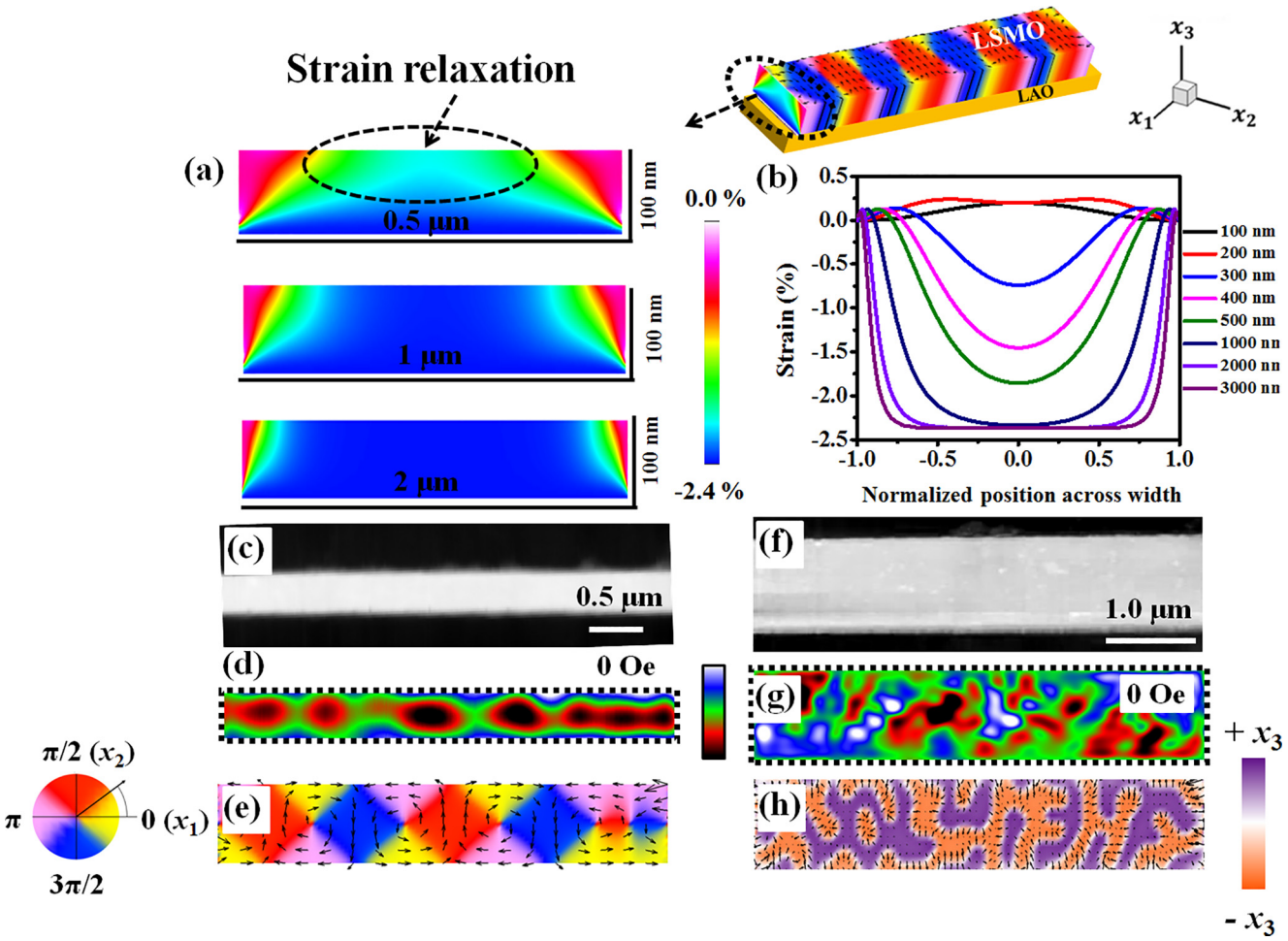

Fig. 2. (Color online) Strain distributions and spin textures in patterned LSMO wires. (a) Cross sectional view (shown in black dotted circle in schematics on top of (b)) of the LSMO lithographically fabricated sample modeled color scale map showing the relaxation of the growth strain as a function of width. (b) Calculated strain profile across the LSMO fabricated samples as a function of the normalized position across the wires of different widths. (c, f) Topography of 0.5 and 1.0 μm wide LSMO wires taken at 4 K using contact mode AFM. (d) MFM image of 0.5 μm wide wire recorded at 4 K after zero field cooling (ZFC) at the same place where the topographic image was taken. (g) MFM image of 1.0 μm wide wire recorded at 4 K in zero field after ZFC. (e, h) Phase field modeling of domains in 0.5 and 1.0 μm wide wires.

magnetic field, the number and the position of vortex change, which can be attributed to the redistribution of the spin arrangements after the magnetization process. Obviously, the appearance of vortices at different positions in the sample gives a clear insight that formation of vortex clusters is not due to internal pinning or defects but a thermally activated random process. The field dependence of the magnetic structure of the 0.5 μm wide sample was further elucidated by phase field modeling (Fig. S8 online), which is in good agreement with experimental observations shown in Fig. 3e. Fig. 3c shows *M-H* curves of 0.5 μm wide wire measured by applying field parallel to length of the wire (red) and parallel to top surface of wire (black). Out-of-plane *M-H* measurements shows complex features which may be due to vortex formation and annihilation. Furthermore, hall resistance measurement ($R_{xy}(H)$) was performed on 0.5 μm wide wire (Fig. 3d). From the $R_{xy}(H)$ loop, while decreasing external magnetic field from saturation, abrupt change in resistance at around ± 1 kOe corresponds to nucleation of vortices; while external field increases above zero in opposite direction, resistance changes gradually as the vortices are forced towards the wire edges as the magnetic moments tends to align parallel with the external field. MFM was also performed on 1.0 μm wide wire in comparison with 0.5 μm wide wire which shows almost similar behavior with thin film. Detailed magnetization reversal process of 1.0 μm wide wire recorded by MFM is shown in Fig. S9 (online).

In order to gain further insights into the evolution of the magnetic order in the presence of different compressive strains, the magnetic phase diagrams of the 0.5 and 1.0 μm wide LSMO wires in terms of ε_{11} and ε_{22} were modeled based on phase-field modeling [29]. The results are shown in Fig. 4. For clarity, the spin textures of the corresponding magnetic orders are given in the right panel of Fig. 4. It can be found that, when subjected to different strains along the ε_1 and ε_2 directions, the LSMO wires can exhibit three different types of magnetic order, namely, the in-plane single domain state, the out-of-plane random domain state, and the vortex cluster state. Furthermore, a triple point of these three states can be observed in this diagram. Our modeling shows that the uniaxial strain relaxation induces a magnetic anisotropy favoring the alignment perpendicular to the wire axis of the one dimensional wire through an inverse magnetostriction effect, while the shape induced anisotropy of the samples prefers to align the magnetization along the wire direction because of the minimization of the stray field. Note that there always exists a compressive strain induced perpendicular anisotropy in the LSMO sample. Therefore, as the width or strain of wires varies, the balance between the uniaxial strain relaxation-, the compressive strain- and the shape-induced anisotropy energy changes, thus giving rise to the rich varieties of the magnetic phases (Fig. 4).

As for the formation of the magnetic vortices in 0.5 μm wide LSMO wires, a detailed calculation shows that with decreasing

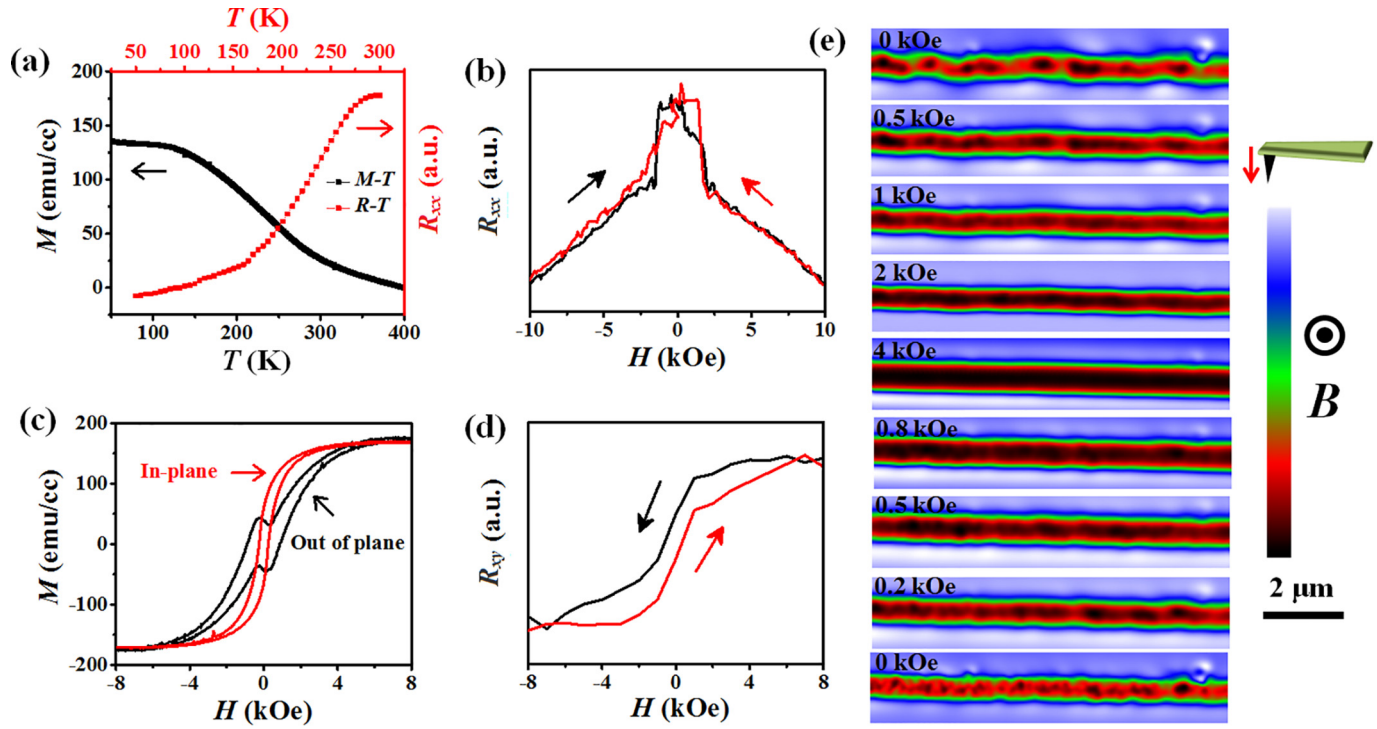

Fig. 3. (Color online) Electrical transport and magnetic domain evolution in a 0.5 μm wide LSMO wire. (a) *M-T* and *R-T* of the 0.5 μm wide wire. (b) $R_{xx}(H)$ taken at 4 K after ZFC. (c) *M-H* loops taken at 4 K after ZFC. (d) $R_{xy}(H)$ taken at 4 K after ZFC. (e) Magnetic field dependent MFM images recorded at 4 K after ZFC which shows vortex annihilation and nucleation process in the 0.5 μm wide wire.

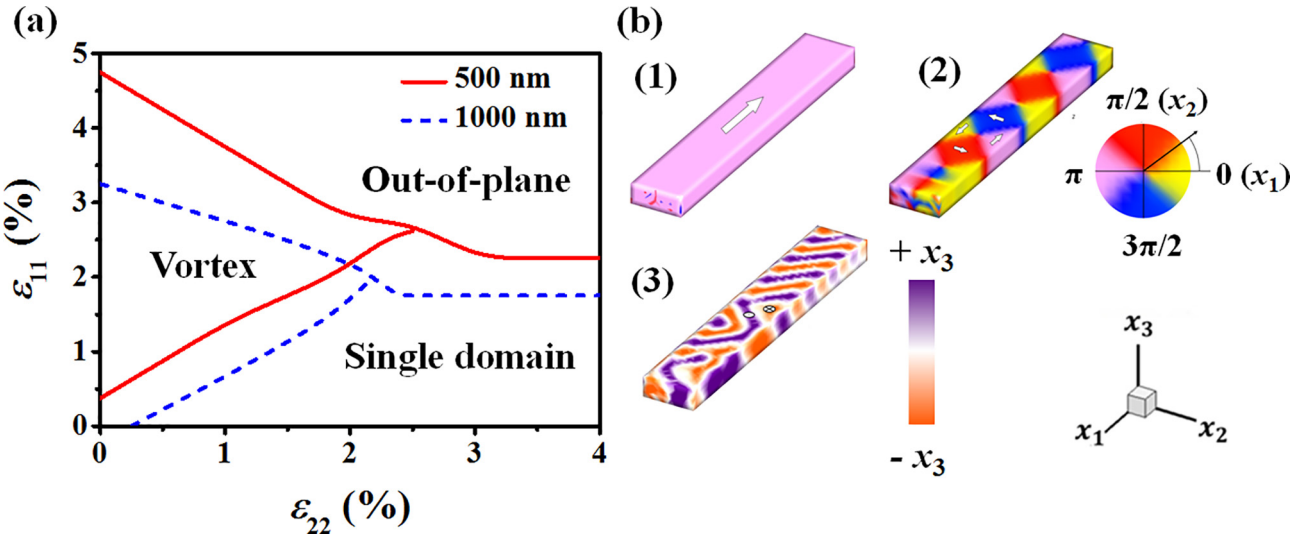

Fig. 4. (Color online) Phase diagram of LSMO in terms of strain in different direction. (a) Phase diagram based on phase field modeling. (b) Magnetic domain configurations at different values of strain. Single magnetic domain with in-plane spin configuration (1), Magnetic vortex clusters with flux closure spin configuration (2) and out-of-plane random domain phase (3).

the wires width, the uniaxial stain relaxation induces anisotropy, which competes fiercely with the shape-induced anisotropy, thus leading to the nonlinear spin textures herein, i.e. the magnetic vortices. Additionally, the modeling also suggests that the complete suppression of the shape-induced anisotropy is disadvantageous for the generation of the magnetic vortices in these samples. This mechanism for the production of the vortex cluster phase can be identified in the phase diagram (Fig. 4). From Fig. 4, it can be found that the vortex clusters state in principle exists in a region where $\varepsilon_{22} < \varepsilon_{11}$ and also $\varepsilon_{22} < 2.37\%$, while the out-of-plane domain state becomes stable under the larger values of both ε_{11} and ε_{22}. This fact confirms that the uniaxial strain relaxation along the $\boldsymbol{x}_2$ direction (manifested by $\varepsilon_{22} < \varepsilon_{11}$) is one of the important reasons for the formation of the vortex cluster phase, whereas the compressive strain that favors the perpendicular anisotropy becomes the dominative mechanism at large value of strain, which accounts for the appearance of the out-of-plane domain state. Additionally, the in-plane single domain state (with spins aligning in the length direction of the wire) exists in the region other than those of the former two phases, which can be attributed to the dominative effect aris-

ing from the shape-induced anisotropy. $\varepsilon_{11} < \varepsilon_{22}$ strain distribution also generates the anisotropy along $\boldsymbol{x}_1$ direction via magnetostrictive effect which supports single domain formation. On the other hand, it is important to note that there is a significant difference between the phase diagrams of 0.5 and 1.0 μm wide wires. That is, compared with that of the 0.5 μm wide sample, the phase boundary, as well as the triple point, of the 1.0 μm wide one performs a shift to the lower left, resulting shrinking of the vortex clusters phase region. As a result, at a fixed ε_{11} of 2.37%, the critical value of ε_{22} corresponding for the phase boundary is ~1.8% for the 1.0 μm sample, significantly lower than that (~2.1%) for the 0.5 μm wide sample. Our modeling shows that the relative weak shaped-induced anisotropy in the 1.0 μm sample compared with that in the 0.5 μm one is the reason for this shrinking of the vortex region. This comparison reveals that the shape induced anisotropy of the wire is also an important factor for the generation of the vortex phase. Certainly, a dominating ultra-strong shape-induced anisotropy in much narrower wires can also have a detrimental effect on the vortex structure, which is evidenced by our calculation showing that the 0.2 μm wide wire only exhibits a single domain state in the same situation. Therefore, the phase diagram in Fig. 4 supports the conclusion that the coexistence and the competition between uniaxial strain relaxation- and shape-induced anisotropies play the dominative role for the stabilization of the magnetic vortex clusters phases, which is different from the reported mechanism in the high symmetric devices wherein the shape induced anisotropy is the only critical factor for the formation magnetic vortex. According to Fig. 2, considering the differences in the strain relaxation along the $\boldsymbol{x}_2$ direction in the realistic systems, modeled magnetic structures of 0.5 and 1.0 μm wide wires are consistent with the results shown in Fig. 4.

4. Conclusions

In conclusion, we report a study of magnetic states of patterned one-dimensional LSMO wires. Interestingly, as the width of the wires decreases from 1.0 to 0.5 μm, a distinctive transformation from an out-of-plane magnetic domain state to magnetic vortex clusters with flux closure spin configuration is observed using VT-MFM at 4 K. Furthermore, the presence of the magnetic vortex cluster phase in 0.5 μm wide wire was also corroborated by magnetoresistance measurement. Based on the phase field modeling, we propose that the enhancement of the uniaxial strain relaxation-induced magnetic anisotropy in narrow wires and its competition with the shape-induced anisotropies plays an important role in stabilizing the flux closure spin structure. This work offers a new perspective for both understanding and manipulation of the non-trivial spin texture in correlated electron, which could be useful for high density data storage devices with strain mediated tunability. Above all, this work demonstrates that the manganite wires can exhibits a vortex clusters phase that is highly tunable through geometric size and the strain in different directions crystallographic axis. This could be useful in future applications based on the novel topological magnetic structures in the correlated oxides.

Conflict of interest

The authors declare that they have no conflict of interest.

Acknowledgments

This work was financially supported by the National Key Research and Development Program of China (2016YFA0302300), the Beijing Natural Science Foundation (Z190008) and the National Natural Science Foundation of China (11974052 and 11474024). J. X. acknowledges the Beamline 1W1A of the Beijing Synchrotron Radiation Facility. X. W. acknowledges the National Natural Science Foundation of China (11604011) and Beijing Institute of Technology Research Fund Program for Young Scholars. J. W. acknowledges the National Natural Science Foundation of China (11672264 and 11621062). The group in Mainz acknowledges support by the German Research Foundation DFG SFB TRR173 Spin + X, project KL1811/18 and the Graduate School of Excellence Materials Science in Mainz (GSC266). The work in Peking University was supported by the National Key R&D Program of China (2016YFA0300804), the National Natural Science Foundation of China (11974023 and 51672007), and the Key R&D Program of Guangdong Province (2018B030327001 and 2018B010109009). P. G. acknowledges Electron Microscopy Laboratory of Peking University for the use of Cs corrected electron microscope.

Author contributions

Jinxing Zhang and Iftikhar Ahmed Malik conceived the experiments and prepared the manuscript. Jing Wang, Yuelin Zhang, Simone Finizio, and Mathias Kläui prepared the samples (Thin films and lithographically fabricated wires). Muhammad Abdullah Malik and Irfan Ahmed performed the XRD and electric characterizations. Iftikhar Ahmed Malik and Rizwan Ullah carried out the SQUID measurement. Houbing Huang, Yu. Wang, Cui Xiao, and Jie Wang provided phase field modeling. Iftikhar Ahmed Malik and Xueyun Wang performed the AFM and MFM measurements. Yuanwei Sun and Peng Gao performed HAAD-STEM and EDX measurements. Jinxing Zhang, Changmin Xiong, Mathias Kläui, Jie Wang and Iftikhar Ahmed Malik were involved in the discussion and revision of the manuscript. All authors were involved in the analysis of the experimental and theoretical results.

Appendix A. Supplementary materials

Supplementary materials to this article can be found online at https://doi.org/10.1016/j.scib.2019.11.025.

References

[1] Parkin SS, Hayashi M, Thomas L. Magnetic domain-wall racetrack memory. Science 2008;320:190–4.
[2] Nagai T, Yamada H, Konoto M, et al. Direct observation of the spin structures of vortex domain walls in ferromagnetic nanowires. Phys Rev B 2008;78:180414.
[3] Wachowiak A, Wiebe J, Bode M, et al. Direct observation of internal spin structure of magnetic vortex cores. Science 2002;298:577–80.
[4] Pribiag V, Krivorotov I, Fuchs G, et al. Magnetic vortex oscillator driven by dc spin-polarized current. Nat Phys 2007;3:498–503.
[5] Rößler UK, Bogdanov AN, Pfleiderer C. Spontaneous skyrmion ground states in magnetic metals. Nature 2006;442:797–801.
[6] Mühlbauer S, Binz B, Jonietz F, et al. Skyrmion lattice in a chiral magnet. Science 2009;323:915–9.
[7] Nagaosa N, Tokura Y. Topological properties and dynamics of magnetic skyrmions. Nat Nanotechnol 2013;8:899–911.
[8] Zang J, Mostovoy M, Han JH, et al. Dynamics of skyrmion crystals in metallic thin films. Phys Rev Lett 2011;107:136804.
[9] Everschor-Sitte K, Masell J, Reeve RM, et al. Perspective: magnetic skyrmions—overview of recent progress in an active research field. J Appl Phys 2018;124:240901.
[10] Malozemoff A, Slonczewski J. Magnetic domain walls in bubble materials. New York 1979; 382.
[11] Hubert A, Schäfer R. Magnetic domains: the analysis of magnetic microstructures. Springer Science & Business Media; 2008.
[12] Moriya T. Anisotropic superexchange interaction and weak ferromagnetism. Phys Rev 1960;120:91–8.
[13] Dennis C, Borges R, Buda L, et al. The defining length scales of mesomagnetism: a review. J Phys Cond Matt 2002;14:R1175–262.
[14] Shinjo T, Okuno T, Hassdorf R, et al. Magnetic vortex core observation in circular dots of permalloy. Science 2000;289:930–2.
[15] Choe S-B, Acremann Y, Scholl A, et al. Vortex core-driven magnetization dynamics. Science 2004;304:420–2.

[16] Uhlíř V, Urbánek M, Hladík L, et al. Dynamic switching of the spin circulation in tapered magnetic nanodisks. Nat Nanotechnol 2013;8:341–6.
[17] Haghiri-Gosnet A, Renard J. CMR manganites: physics, thin films and devices. J Phys D Appl Phys 2003;36:R127–50.
[18] Uehara M, Mori S, Chen C, et al. Percolative phase separation underlies colossal magnetoresistance in mixed-valent manganites. Nature 1999;399:560–3.
[19] Jin S, Tiefel TH, McCormack M, et al. Thousandfold change in resistivity in magnetoresistive $LaCaMnO_3$ films. Science 1994;264:413–5.
[20] Wang J, Xie L, Wang C, et al. Magnetic domain-wall motion twisted by nanoscale probe-induced spin transfer. Phys Rev B 2014;90:224407.
[21] Liu C, Wu S, Zhang J, et al. Current-controlled propagation of spin waves in antiparallel, coupled domains. Nat Nanotechnol 2019;14:691–7.
[22] Vistoli L, Wang W, Sander A, et al. Giant topological hall effect in correlated oxide thin films. Nat Phys 2019;15:67–72.
[23] Suzuki Y, Hwang H, Cheong S, et al. The role of strain in magnetic anisotropy of manganite thin films. Appl Phys Lett 1997;71:140–2.
[24] Reeve RM, Mix C, König M, et al. Magnetic domain structure of $La_{0.7}Sr_{0.3}MnO_3$ thin-films probed at variable temperature with scanning electron microscopy with polarization analysis. Appl Phys Lett 2013;102:122407.
[25] Cui B, Song C, Gehring GA, et al. Electrical manipulation of orbital occupancy and magnetic anisotropy in manganites. Adv Func Mat 2015;25:864–70.
[26] Wang J, Wu S, Ma J, et al. Nanoscale control of stripe-ordered magnetic domain walls by vertical spin transfer torque in $La_{0.7}Sr_{0.3}MnO_3$ film. Appl Phys Lett 2018;112:072408.
[27] Quacquarelli FP, Puebla J, Scheler T, et al. Scanning probe microscopy in an ultra-low vibration closed-cycle cryostat. Microsc Today 2014;23:12–7.
[28] Song C, Malik IA, Li M, et al. Hidden metal-insulator transition in manganites synthesized via a controllable oxidation. Sci China Mater 2018;62:577–85.
[29] Wang J, Zhang J. A real-space phase field model for the domain evolution of ferromagnetic materials. Int J Solids Struc 2013;50:3597–609.
[30] Kwon C, Robson M, Kim K-C, et al. Stress-induced effects in epitaxial $(La_{0.7}Sr_{0.3})MnO_3$ films. J Magn Magn Mater 1997;172:229–36.
[31] Endo M, Kanai S, Ikeda S, et al. Electric-field effects on thickness dependent magnetic anisotropy of sputtered $MgO/Co_{40}Fe_{40}B_{20}/Ta$ structures. Appl Phys Lett 2010;96:212503.

Iftikhar Ahmed Malik is a Ph.D. candidate in Jinxing Zhang group, at Department of Physics, Beijing Normal University. His research focuses on the static and dynamic properties of geometrically confined spin structures, and spin transfer torque as well as current-induced manipulation of non-linear spin textures using Cryo-Temperature scanning probe microscopy. In addition, manipulating the phase coexistence state in complex oxides and providing insight into the size limitation for designing next generation electronic/spintronic devices is his research interest.

Changmin Xiong received his Ph.D. degree in Condensed Matter Physics in 2005 from Institute of Physics, Chinese Academy of Sciences, China. Since 2009, he has been an associate professor at Department of Physics, Beijing Normal University, China. His research focuses on the fabrication and understanding of the magnetic materials and complex oxides heterojunction.

Jie Wang is a Professor in the Department of Engineering Mechanics at Zhejiang University. He received his bachelor degree from Xi'an Jiaotong University in 1998, Master degree from Lanzhou University in 2002, and Ph.D. degree from the Hong Kong University of Science and Technology (HKUST) in 2006. His research mainly focuses on the first-principle calculations and phase field modeling on the multi-field coupling properties of ferroelectric, ferromagnetic and multi-ferroic materials.

Jinxing Zhang obtained his Ph.D. degree from The Hong Kong Polytechnic University in 2009. In 2012, he joined the Department of Physics, Beijing Normal University as a professor. His team is striving to create a bridge between those fundamentally scientific discoveries in functional nano-systems and future possible applications such as sensing, actuation, data storage, energy conversion, quantum manipulation, etc.